applied sciences

MDPI

Article

Time Domain Investigation of Hybrid Intelligent Controllers Fed Five-Phase PMBLDC Motor Drive

M. A. Inayathullaah [1,*], N. Sivakumar [2], Ananthakrishnan Balasundaram [3,4], R. Arul [1] and S. Angalaeswari [1]

[1] School of Electrical Engineering, Vellore Institute of Technology, Chennai 600127, India
[2] Department of Engineering Management, St. Cloud State University, St. Cloud, MN 563014498, USA
[3] Centre for Cyber Physical Systems, Vellore Institute of Technology, Chennai 600127, India
[4] School of Computer Science and Engineering, Vellore Institute of Technology, Chennai 600127, India
* Correspondence: inayathullah.a@vit.ac.in

Abstract: This paper presents a modeling and performance evaluation of a five-phase PMBLDC motor with different controllers to analyze its transients and dynamic response with time domain specifications. Four different types of speed controllers, namely an Adaptive Neuro-Fuzzy Inference System (ANFIS), an Adaptive Hybrid fuzzy-PI, a Proportional Integral (PI) control and a Fuzzy Logic Control (FLC), were considered and compared for this purpose. The mathematical model of the five-phase Permanent Magnet Brushless Direct Current (PMBLDC) motor was developed and simulated using MATLAB/Simulink to analyze its performance. The simulation results for all controllers with step and linear load fluctuations were evaluated. It was evident that the ANFIS controller provided a better dynamic time domain response than the other controllers. It gave eight times the peak torque at starting, and settled at 92.6% of the rated speed, with negligible overshoot, a very low rise time and a quick settling time compared to other controllers, which are ideally suited for an electric vehicle (EV). A real-time experimental setup was also developed, and experiments were carried out to validate the simulation results.

Keywords: Brushless DC motors (BLDC); five-phase; Permanent Magnet (PM) motor; fuzzy logic controller; proportional plus Integral controller (PI); ANFIS controller; hybrid fuzzy-PI

check for updates

Citation: Inayathullaah, M.A.; Sivakumar, N.; Balasundaram, A.; Arul, R.; Angalaeswari, S. Time Domain Investigation of Hybrid Intelligent Controllers Fed Five-Phase PMBLDC Motor Drive. *Appl. Sci.* **2023**, *13*, 3281. https://doi.org/10.3390/app13053281

Academic Editor: Alexander S. Semenov

Received: 25 January 2023
Revised: 22 February 2023
Accepted: 23 February 2023
Published: 4 March 2023

Copyright: © 2023 by the authors. Licensee MDPI, Basel, Switzerland. This article is an open access article distributed under the terms and conditions of the Creative Commons Attribution (CC BY) license (https://creativecommons.org/licenses/by/4.0/).

1. Introduction

Multi-phase machines have increased in terms of their visibility in recent years due to their low torque ripples, good fault tolerance capability, use of low ratings switches and high torque/current ratio [1]. Multiphase machines are machines with more than three phase windings for creating a rotating torque [2]. With a power electronic converter, the number of phases is virtually not limited, and multi-phase machines are potentially viewed as suitable solutions for high current and power applications [3]. However, in comparison with three-phase drives, multiphase drives provide quite a lot of edges in the utilization of low power consumption, they are highly reliable and they have low dc-link voltage [4]. The significant benefits of multiphase motors drives are: (a) a higher reliability and superior fault tolerance capability; (b) a low amplitude and increased frequency of torque pulsations; (c) low per phase power handling; (d) better modularity; (e) advanced noise characteristics; and (f) less dc-link current harmonics. In multi-phase drives, as the number of devices and gate drives increases, the possibility of faults as well as costs increases, which no longer justifies the marginal increase in performance; hence, the optimum number of phases with good optimization is to be considered as five [5–9].

Compared to conventional three-phase PM motors, five-phase PM motors possess the advantage of having a higher torque density per ampere of stator current, with lower stator current per phase at the same voltage level. Hence, multiphase motor drives are highly appropriate for applications such as marine electric vehicles (EVs), locomotive traction, electric propulsion and hybrid electric vehicles (HEVs), as well as low power and high

torque applications in general. The focus of researchers has migrated to five-phase PMBLDC motors over three-phase PMBLDC motors due to their fault tolerance capabilities [10–12]. Consider the case of a three-phase PMBLDC motor driving a mechanical load. In a three-phase star-connected stator-winded BLDC motor connected to a load, while switching, one phase will always be ideal, and the remaining series connected to two phases will carry the load current. Due to overload, or short circuiting in the windings, if the working phase is opened, the motor suddenly drops to zero speed, ignoring the load demand at a given time. This results in poor load regulation and zero tolerance capability [13–15].

Five-phase motors overcome this issue in conventional three-phase motors and provide good reliability. In five-phase motors under a faulty phase, the remaining three phases can still drive the load and the drive needs not be instantly halted [16,17]. The occurrence of torque ripple in three-phase PMBLDC motors is considered a significant worry in applications where position and speed control accuracy are of great significance, and for which the five-phase counterparts are the only solution. PI controller-based PMBLDC motors have a better performance than fuzzy logic controllers do in a steady state than transients [18]. Despite this, the design of a PI controller requires a mathematical model of the motor with a high degree of accuracy. The FLC controller does not depend on an accurate mathematical model of the motor; and hence, it effectively substitutes the PI controller, as it is a rule-based linguistic controller. Still, the performance of the fuzzy controller is only better under transient conditions, but not in a steady state condition [18–20].

An adaptive hybrid fuzzy-PI controller combines the benefits of the fuzzy and PI controllers in both steady state and transient conditions [21,22]. One of the main shortcomings of FLC is the presence of the trial-and-error process in the identification of fuzzy rules, the fuzzy membership function [23,24], and their definitions, along with the universe of discourse. To overcome this, the controller must adapt itself to changes in plant dynamics. This can be achieved with the ANFIS controller. The selection of the rule base, based on the situation based on trained neural network techniques, is used in the ANFIS controller; and hence, this approach to control yields excellent results [25–27].

The fault tolerance capability of multiphase motors has been discussed in [28], and various speed controller techniques applied to three-phase PMBLDC motors have been discussed in [29–32]. After going through all of the above literature, it is understood that the time domain analysis of five-phase PMBLDC motors with multiple speed controllers has not been discussed by researchers. Moreover, the testing of the dynamic and steady state performance of BLDC motor drives for electric vehicle applications has been restricted to three-phase machines in the literature under no load and load conditions [33–41]. There has been no similar work carried out for multi-phase/five-phase BLDC motors so far. Hence, the proposed work carried out in this paper uses different load conditions applied to different controller-fed drives, and their performance characteristics are discussed.

In this context, the design and performance evaluation of conventional and intelligent controllers are analyzed and compared for five-phase PMBLDC motor drives in terms of time domain specifications under different load conditions in this paper, as shown in Figure 1. The simulation results show that the ANFIS controller-based five-phase PMBLDC motor drive system has the benefits of low torque ripples, a high starting torque, a better transient response along with negligible overshoot, and a smaller rise and settling time, which make it ideally suited for electric vehicle applications.

The rest of this paper is organized as follows: Section 2 describes the mathematical model of five-phase PMBLDC motor drives. Section 3 describes the design aspects of different controllers for the modeled drive. Section 4 explains the simulation of the drive with step and linear load variations. The experimental setup and corresponding results are described in Section 5. The conclusions of this paper are given in Section 6.

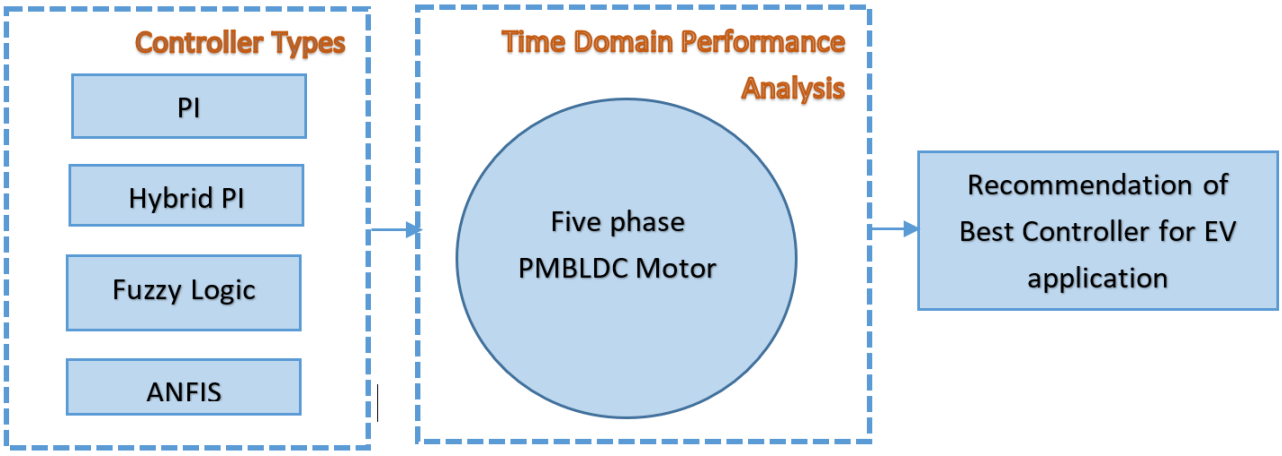


Figure 1. Technical drawing of the proposed work.

2. Modeling of Five-Phase PMBLDC Motor Drive SYSTEM

There are different methods for modeling a PMBLDC motor, but when it is needed to study time domain characteristics, only time domain modeling is preferred, which has been carried out in this paper for the proposed multiphase machine.

The modeling of the five-phase Permanent Magnet BLDC motor as based on the electrical equivalent circuit diagram shown in Figure 2b. Figure 2a,b depicts both the entire drive system configuration of the proposed motor drive and its mathematical motor model. The pulse width modulation (PWM)-based inverter has a ten-switch, five-leg voltage source configuration energized with a fixed dc-link voltage (V_d).

The following list of assumptions were made for simplifying the analysis.

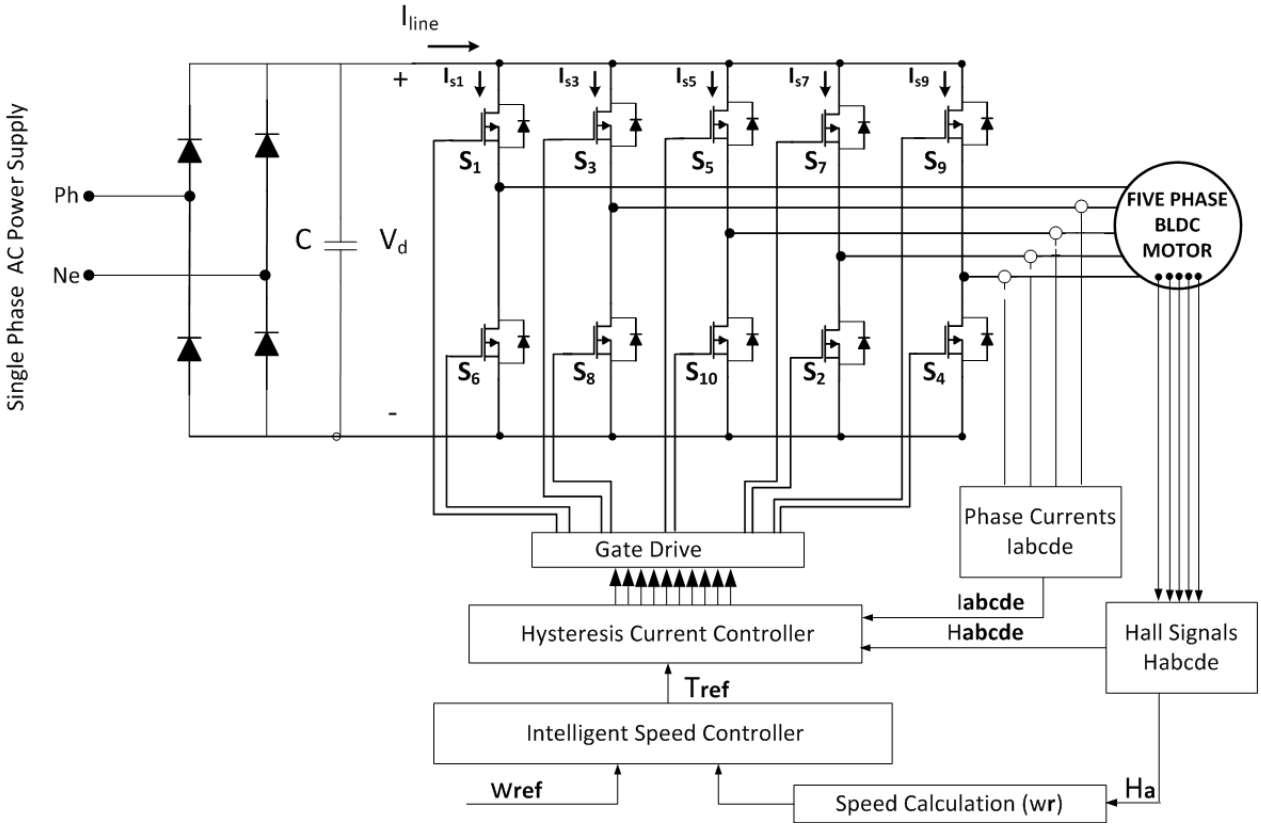
- The stator field winding is unsaturated;
- Stator per phase resistance in all the windings is the same;
- Mutual and self-inductances are fixed;
- Ideal power semiconductor switches in the inverter;
- Negligible iron losses.

A delta-connected five-phase PMBLDC motor incorporating the above assumptions is represented in phase variable model as,

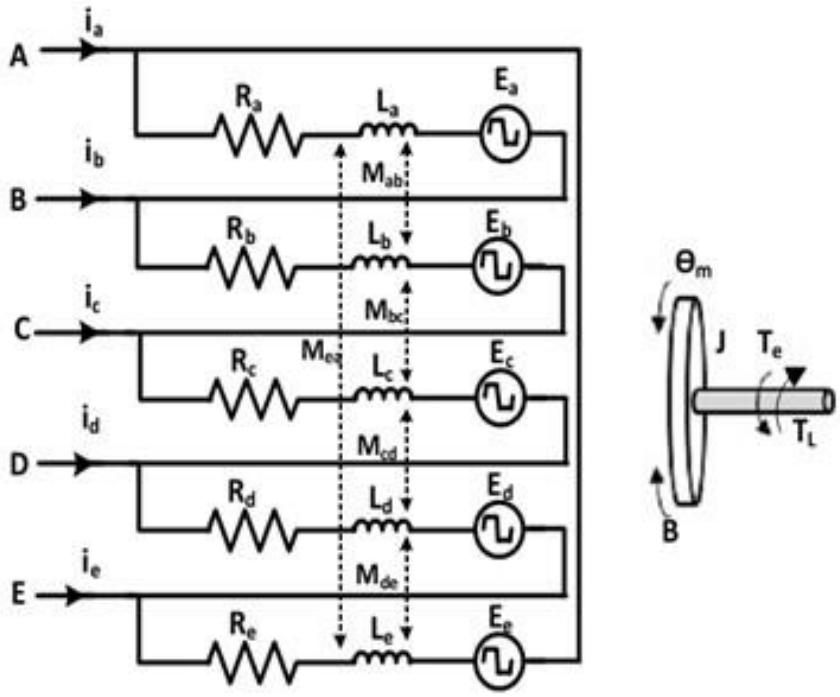
$$\begin{bmatrix} V_{ab} \\ V_{bc} \\ V_{cd} \\ V_{de} \\ V_{ea} \end{bmatrix} = R_S \begin{bmatrix} i_a - i_b \\ i_b - i_c \\ i_c - i_d \\ i_d - i_e \\ i_e - i_a \end{bmatrix} + L_S \frac{d}{dt} \begin{bmatrix} i_a - i_b \\ i_b - i_c \\ i_c - i_d \\ i_d - i_e \\ i_e - i_a \end{bmatrix} + \begin{bmatrix} E_a - E_b \\ E_b - E_c \\ E_c - E_d \\ E_d - E_e \\ E_e - E_a \end{bmatrix} \quad (1)$$

where, V, L, M, i, and E, represent the line-to-line voltage, self-inductance, mutual inductance, current, and back emf of the corresponding five phases a, b, c, d, and e, respectively. Considering the phase resistances of each phase are balanced and equal, the effective line-to-line resistance Rs is expressed as Rs = 2R in ohm.

$$\begin{gathered} R_a = R_b = R_c = R_d = R_e = R\,; L_a = L_b = L_c = L_d = L_e = L\,; \\ M_{ab} = M_{bc} = M_{cd} = M_{de} = M_{ea} = M\,; \\ i_a = i_b = i_c = i_d = i_e \;; M_{ib} + M_{ic} + M_{id} + M_{ie} = -M_{ia} \end{gathered} \quad (2)$$



(**a**)



(**b**)

Figure 2. Five-phase PMBLDC motor drive and its motor's electrical model. (**a**) Five-leg MOSFET inverter-fed BLDC motor drive. (**b**) Equivalent electrical model of the motor.

Incorporating Equation (2) into Equation (1), and after simplifying, we obtain the equation in a state space form as (3), and implement it in a MATLAB Simulink environment,

$$\frac{d}{dt}\begin{bmatrix} i_a - i_b \\ i_b - i_c \\ i_c - i_d \\ i_d - i_e \\ i_e - i_a \end{bmatrix} = \frac{1}{L_s}\left[\begin{bmatrix} V_{ab} \\ V_{bc} \\ V_{cd} \\ V_{de} \\ V_{ea} \end{bmatrix} - R_S \begin{bmatrix} i_a - i_b \\ i_b - i_c \\ i_c - i_d \\ i_d - i_e \\ i_e - i_a \end{bmatrix} - \begin{bmatrix} E_a - E_b \\ E_b - E_c \\ E_c - E_d \\ E_d - E_e \\ E_e - E_a \end{bmatrix}\right] \tag{3}$$

The mechanical part of the motor is the process of electromagnetic torque production, and the equation governing this process is given by,

$$T_e = T_L + J\frac{d\omega}{dt} + B\omega \tag{4}$$

where TL denotes load torque (Nm), J denotes moment of inertia (Kgm^2), and B denotes damping coefficient of friction in (Nms/rad). The equations are used to construct the Simulink model of the five-phase PMBLDC motor drive in the MATLAB environment.

3. Design of Controllers

The dynamic and transient behavior of PMBLDC motors is determined by the proper design of controllers. Care should be taken in deciding the controller parameters to suit low torque high power applications. The controllers, which have been used for this analysis, are discussed below.

3.1. PI Controller

The model of the PI speed controller in the frequency domain is given by

$$G(s) = K_p + \frac{K_i}{s} \tag{5}$$

where the transfer function of the controller is given by G(s), the proportional gain constant is denoted by K_p, and the integral gain constant is denoted by K_i. The Ziegler-Nichols method [32] is used for the tuning of these parameters to ensure stability. The transient behavior of the speed response gives the time domain specifications, such as peak time (T_p); percentage overshoots (M_p), settling time (T_s), and rise time (T_r). The closed-loop second-order transfer function for the proposed five-phase PMBLDC motor with the PI controller is given as,

$$(s) = \frac{\frac{K_p s + K_i}{J}}{s^2 + \frac{B+K_p}{J}s + \frac{K_i}{J}} \tag{6}$$

where T(s) is the closed-loop transfer function of the entire system, J denotes moment of inertia, and B denotes coefficient of friction of the PMBLDC motor. Comparing the characteristic Equation (6) with that of a standard second-order system characteristic, we obtain Equation (7) providing the gain constants as,

$$Kp = 2\xi\omega n\ J\text{-}B;\ Ki = J\omega n2 \tag{7}$$

3.2. Fuzzy Logic Controller

The fuzzy logic controller helps the designer to linguistically express the general characteristics of any non-linear system by forming IF-THEN rules. The fuzzy logic controller consists of four functional blocks, namely fuzzification, defuzzification, fuzzy inference engine, and fuzzy rule-base. A triangular membership function for input parameters, namely error (M) and change in error (ΔM), has been considered. Similarly, for the output parameter, a torque reference (T_{ref}) is considered with the same type of triangular membership.

The Fuzzy Associate Memories (FAM), as given in Table 1, depict the rules of the fuzzy logic controller. Based on the literature review on the selection of FAM, for simplicity and accuracy, we chose a triangular-shaped membership function with a 50% overlapping rate for fuzzy linguistic sets, namely Negative Large (NL), Negative Medium (NM), Negative Small (NS), Zero (Z), Positive Large (PL), Positive Medium (PM), and Positive Small (PS). This function is used for both the input variable, namely, error (M) and change in error (ΔM), as well as the output variable, namely, the torque reference (T_{ref}). The final fuzzy output (T_{ref}) is converted into a crisp output using the Centroid method of defuzzification process,

$$Z = \frac{\sum_{x=1}^{n} \mu(x)x}{\sum_{x=1}^{n} \mu(x)} \quad (8)$$

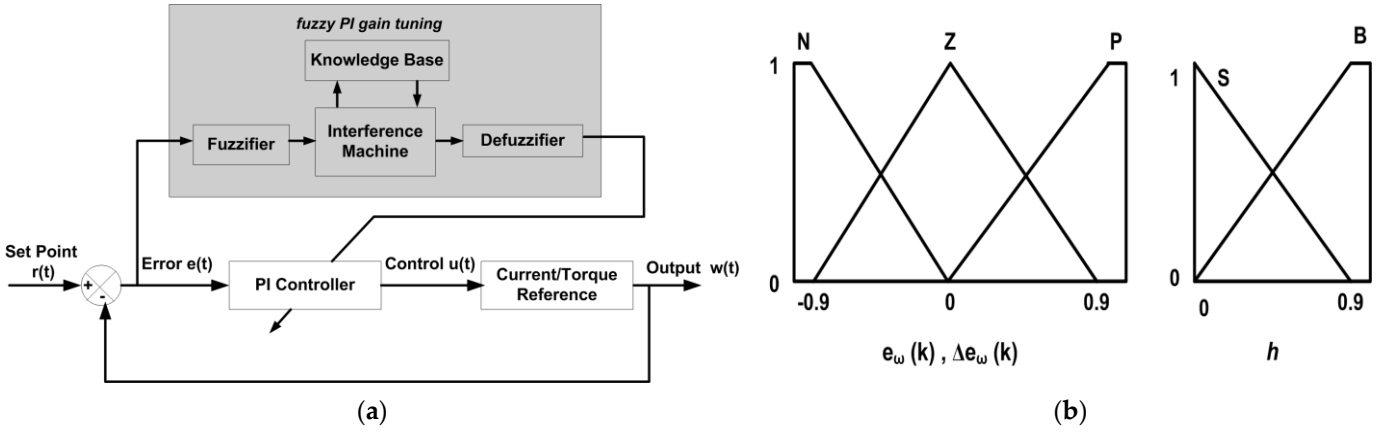
where Z is the defuzzified value, and μ(x) is the membership value of member x.

Table 1. Fuzzy Associative Memory Table.

ΔM \ M	NL	NM	NS	Z	PS	PM	PL
NL	NL	NL	NL	NM	NS	NS	Z
NM	NL	NM	NM	NM	NS	Z	PS
NS	NL	NM	NS	NS	Z	PS	PM
Z	NL	NM	NS	Z	PS	PM	PL
PS	NM	NS	Z	PS	PS	PM	PL
PM	NS	Z	PS	PM	PM	PM	PL
PL	Z	PS	PS	PM	PM	PL	PL

3.3. Adaptive Hybrid Fuzzy-PI Controller

The conventional fixed gain PI controller cannot provide good response for all operating conditions due to the fixing of Kp and Ki values, irrespective of test conditions. Therefore, the proportional and integral constants should be adjusted online to obtain a better transient and steady state response. The adaptive hybrid controller, along with the fuzzy membership function, is depicted in Figure 3; the fuzzy logic controller tunes the constants of the PI controller, Kp, and Ki online. The fuzzy input sets are error (e) and change in error (Δe), which are taken as a triangular function. The linguistic variables are negative (N), zero (Z), and Positive (P). The fuzzy output sets are the tunable parameter (h) with a triangular membership function. Big (B) and small (S) are the linguistic variables. A total of nine rules were framed based on expert knowledge.



(**a**) (**b**)

Figure 3. Adaptive Fuzzy-PI controller. (**a**) Structure of Adaptive Hybrid Fuzzy-PI Controller. (**b**) Membership Function.

The values of Kp and Ki for the hybrid adaptive controllers are obtained [34] from the following:

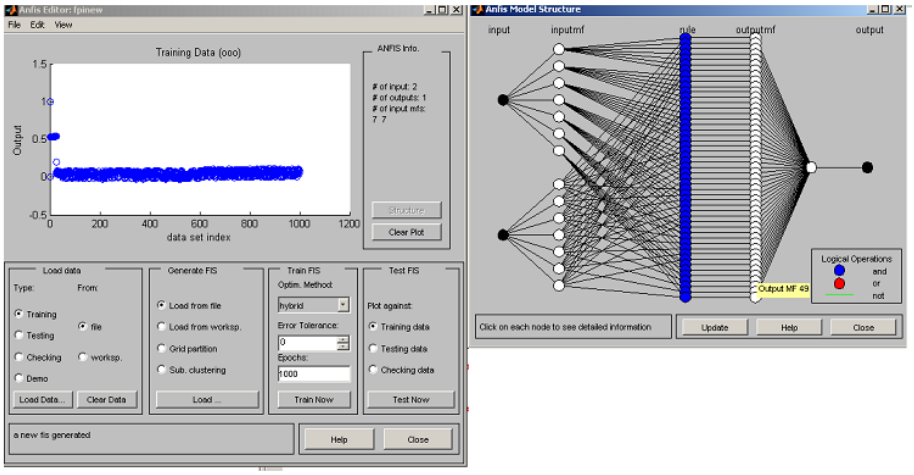
$$Kp = h\ Kpm;\ Ki = h2\ Kim;\ 0.0 < h \leq 1.0 \quad (9)$$

where Kpm and Kim are the maximum possible proportional and integral constants obtained from the Ziegler-Nichols method, respectively, and 'h' is an empirical constant. Here, the value of the PI controller has been tuned online according to the current error using a fuzzy controller.

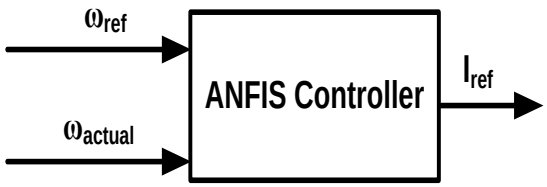
3.4. ANFIS Controller

The design and simulation of the ANFIS controller was carried out by using the software MATLAB R2014a. The 'anfisedit' command initiates the design process by opening the ANFIS GUI editor window for one input, and one output with three membership functions for each variable by default. The sampled data using the 'load data' option from a file are loaded.

The data file contains the information of error, change in error, and expected fuzzified output. Once the data file is loaded, the ANFIS structure changes to two inputs and one output five-layer feed forward fuzzy neural network. The 'generate FIS' option defines the number of input and output membership functions and creates the FIS for the ANFIS controller. Seven triangular input membership functions are selected for both the input and output, completing the initializing stage. The ANFIS logic and structure of the ANFIS controller are shown in Figure 4. The training of neural networks has been carried out by a hybrid algorithm combining the least squares (forward pass) method and the gradient descent (backward pass) method with 1000 epochs or iterations [35]. After the completion of the training, if the error of practice is within the error tolerance, the ANFIS structure has been written and saved. Thus, the designed ANFIS file was used by the fuzzy logic controller to evaluate the effectiveness of the ANFIS controller during a simulation.



(**a**)



(**b**)

Figure 4. Simulation view of ANFIS controller. (**a**) Structure of ANFIS controller with its membership function. (**b**) ANFIS logic.

4. Simulation and Discussion

The simulation of the entire system was carried out in the MATLAB 8.3 Simulink environment. The PI speed controller, fuzzy controller, adaptive hybrid fuzzy-PI controller, and ANFIS controller-based simulation of the five-phase PMBLDC motor drive were designed using its mathematical model. The Simulink view of the ANFIS speed controller was implemented to drive a five-phase PMBLDC motor, as shown in Figure 5. The FIS system was developed using the file fpinew. The tuned values of the proportional gain constant Kp = 1/800 and the Integral gain Ki = 1/200 were found using the Ziegler-Nichols method.

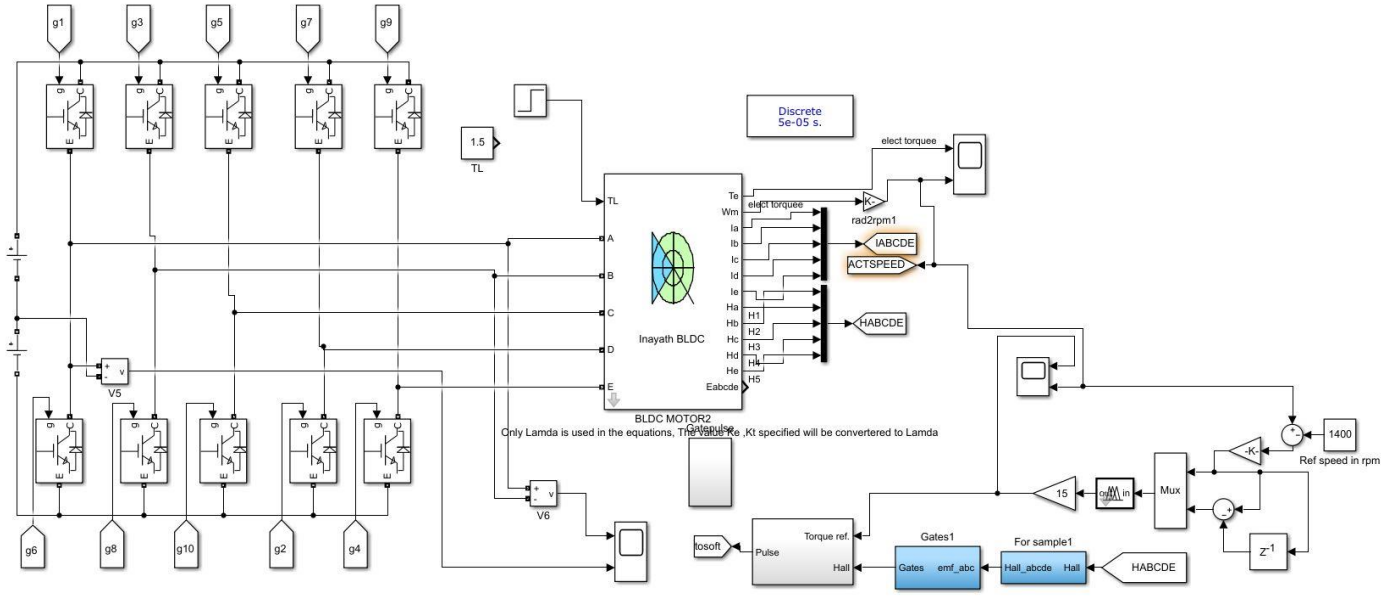


Figure 5. ANFIS speed controller of five-phase PMBLDC drive- Simulink layout.

The simulation was carried out for two different loading conditions, such as step load variation and linear load variation, as discussed in [25].

4.1. Load Variation Characteristics

4.1.1. Step Load Variation

The motor is started with no load from zero seconds. It is allowed to achieve its steady state rated speed of 1400 rpm. The motor attains this speed from 0 to 1 s. At 1 s, a load torque of 2 nm is suddenly applied from 1 to 1.2 s. This maximum load torque is more than the rated load torque of 1.5 nm. At 3.3 s, the load torque is suddenly removed and the motor is allowed to run on no load from 3.5 s to 5 s.

4.1.2. Linear Load Variation

The motor is started with no load from 0 to 1 s. The motor is gradually loaded from 1 to 2.5 s for a varying torque of 0 to 2 nm. The peak load torque of 2 nm is maintained from 2.5 s to 3.5 s. After 3.5 s, the load is gradually removed from 2 to 0 nm for 1 s. The motor is driven at no load from 4.5 to 5 s.

4.2. PI Controller Drive

The response curves of the proposed drive with a PI controller are depicted in Figure 6 and summarized in Table 2.

4.2.1. Starting Characteristics

For a small period of time, the torque rises to 7 nm before returning to its reference value at 0 nm. When the motor is turned on with no load, the percentage overshoot is

22.5 percent, and the peak time observed is 0.3214 s; the rise time observed is 0.1069 s, and the settling time observed is 0.4350 s. In both types of load variations, the results of the simulation carried out from t = 0 s to t = 1 s are the same.

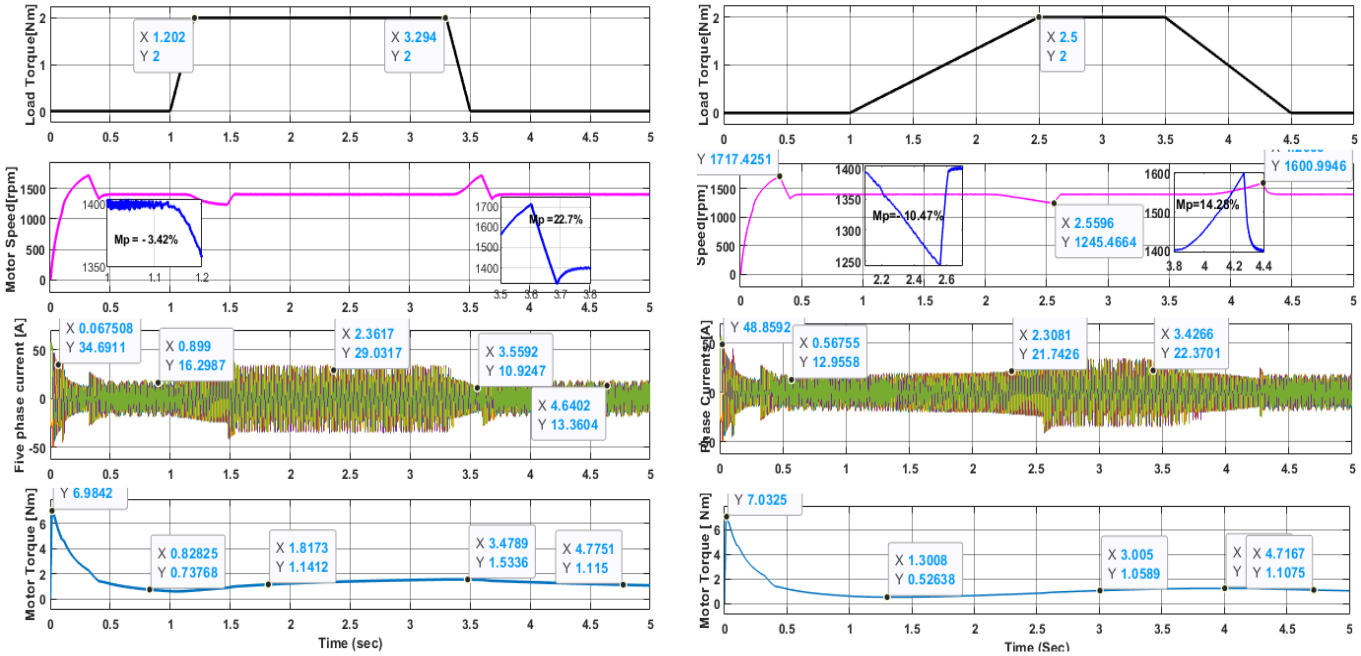


Figure 6. Transient performance of the drive with a PI controller.

Table 2. PI Controller Characteristics.

Load Variation	Characteristics	Time Interval (s)	Overshoot %	Peak Time (s)	Rise Time (s)	Settling Time (s)	Steady State Error
Step load variation	Starting	0–1	22.50	0.3214	0.1069	0.4350	−2 rpm
	Loading	1–1.2	−3.429	1.0056	0.1948	1.1996	42.2 rpm
	Unloading	3.3–3.5	0	3.5	0.00059	3.4989	−163 rpm
	Load removal	3.5–5	22.27	3.6020	0.0288	4.2401	−1.5 rpm
Linear load variation	Starting	0–1	22.50	0.3214	0.1069	0.4350	−2 rpm
	Gradual increases of load	1–2.5	11.11	1.0850	0.3325	2.4838	135 rpm
	Constant Max Load	2.5–3.5	0.4088	3.1671	0.0365	3.4975	2.3 rpm
	Gradual decrease in load	3.5–4.5	14.28	4.2666	0.0216	4.4988	2.8 rpm
	No Load	4.5–5	14.28	4.2666	0.0216	4.4988	2.8 rpm

4.2.2. Step or Gradual Application and Removal of Load

The results indicate that when the step load is applied, it is observed that the settling time is 0.435 s and has a −3.48% overshoot between 1 s to 1.2 s. When the load is removed, the overshoot value is 22.7% (between 3.5 s–3.8 s) with a settling time of 4.2401 s. During the time interval of 1 s to 2.5 s, the load linearly increases from 1 nm to 2 nm with a settling time of 2.4828 s with 135 rpm, having a steady state error and a 10.47% overshoot from 2 s to 3 s. After 2.5 s and up to 3.5 s, when the constant value of 2 nm is applied, the settling time is 3.497 s. Between 3.5 to 4.5 s, the load linearly decreases and it gradually settles down with an overshoot value of 14.28%, with a 2.8 rpm error and a settling time of 4.49 s. At 4.5 s, the load is completely removed until 5 s.

4.3. Fuzzy Controller Drive

The response curves pertaining to the five-phase PMBLDC drive with a fuzzy controller is depicted in Figure 7 and is summarized in Table 3.

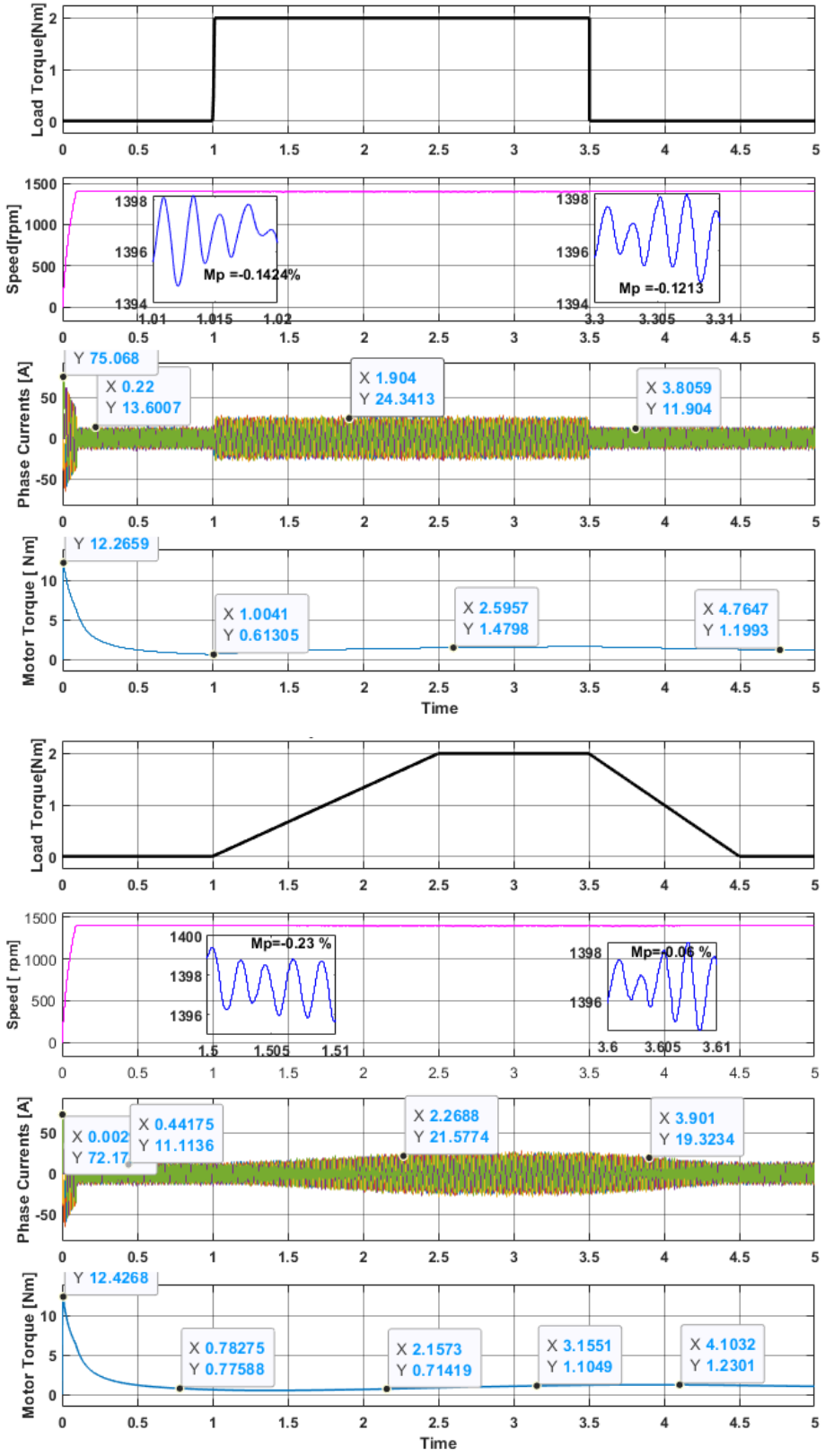


Figure 7. Transient performance of the drive with a fuzzy controller.

4.3.1. Starting Characteristics

The initial torque of the motor is 12 nm, and it is 41.6% more than the PI-controller-driven five-phase BLDC motor. While starting the motor with no load, the overshoot percentage is −0.0722 (99.67% less than the PI controller), the peak time value is 0.7664 s,

the rise time is observed as 0.0697 s, and the observed settling time is 0.0881 s. The simulation result from t = 0 s to t = 1 s is the same across both types of load variations. It is seen that the speed settles at 1398 rpm (2 rpm less), the steady state speed for all load conditions.

Table 3. Fuzzy Controller Characteristics.

Load Variation	Characteristics	Time Interval (s)	Overshoot %	Peak Time (s)	Rise Time (s)	Settling Time (s)	Steady State Error
Step load variation	Starting	0–1	−0.0722	0.7664	0.0697	0.0881	1 rpm
	Loading	1–1.2	−0.1424	1.0003	0.00024	1.2	2 rpm
	Unloading	3.3–3.5	−0.1213	3.3932	0.00025	3.5	3 rpm
	Load removal	3.5–5	−0.1177	3.8204	0.00019	5.0000	2 rpm
Linear load variation	Starting	0–1	−0.0722	0.7664	0.0697	0.0881	1 rpm
	Gradual increases of load	1–2.5	−0.2328	1.0131	0.0026	2.499	3 rpm
	Constant Max Load	2.5–3.5	−0.1517	2.6278	0.000207	3.499	4 rpm
	Gradual decrease in load	3.5–4.5	−0.0679	4.4920	0.1789	4.500	1 rpm
	No Load	4.5–5	−0.0679	4.4920	0.1789	4.500	1 rpm

4.3.2. Applying or Removal of Step or Linear Load

The results indicate that while applying the step load, the observed settling time is 0.0881 s, with a −0.1424% overshoot between 1.01 s to 1.02 s. While removing the load, the overshoot is −0.1213% (between 3.3 s–3.31 s) with a settling time of 4.99 s. When the load is linearly increasing from 1 s to 2.5 s to 2 nm, the settling time is 2.499 s with a 3 rpm steady state error and a −0.23% (1.5 s to 1.51 s) overshoot. After 2.5 s and up to 3.5 s, when the load reaches a steady state value of 2 nm, it has a settling time of 3.499 s. Between 3.5 to 4.5 s, the load linearly decreases and gradually settles with an overshoot of −0.06% with a 1 rpm error and a settling time of 4.5 s.

4.4. Fuzzy-PI Controller Driven Drive

The speed, phase current, and torque response curves of the five-phase PMBLDC drive with fuzzy-PI controller is shown in Figure 8 and summarized in Table 4.

4.4.1. Starting Characteristics

The characteristics of fuzzy-PI will be in between the PI controller and the fuzzy controller. The motor attains a steady state speed of 1400 rpm during starting without any load torque. The torque rises to 10 nm (7 nm for PI, 12 nm for Fuzzy Controller) and settles to its reference value close to 0.6 nm. The percentage overshoot at start with no load is 4.9%, (22.5% for PI, −0.07% for fuzzy controller); the respective peak time, rise time, and settling time are 0.1599 s, 0.0993 s, and 0.1778 s, respectively. The simulation performance at start is the same during step and linear loading conditions.

4.4.2. Step or Gradual Application and Removal of Load

The simulation performance depicts that when a step load is applied from 1 s to 1.2 s, the motor settles to the steady state speed at 1.195 s with a −5.5% (−3.4% for PI, −0.14% for fuzzy controller) overshoot. During unloading at 3.5 s, the overshoot is 5.1%, with a settling time of 4.9 s and a steady-state error of just 2 rpm.

When the load is linearly increasing from 1 nm to 2.5 nm between 1 s to 2.5 s, the settling time is 2.49 s, with a 59 rpm steady state error and a −4.5% (2.1 s to 2.5 s) overshoot. After 2.5 s and up to 3.5 s, the loading is kept constant with 2 nm; in this case, the settling time is 3.49 s. Between 3.5 to 4.5 s, unloading proportionately occurs and the speed settles down with an overshoot of 3.03% (14.28% for PI, −0.06% for fuzzy controller) with a 1 rpm error and a settling time of 4.49 s. After 4.5 s and until 5 s, the load is completely removed.

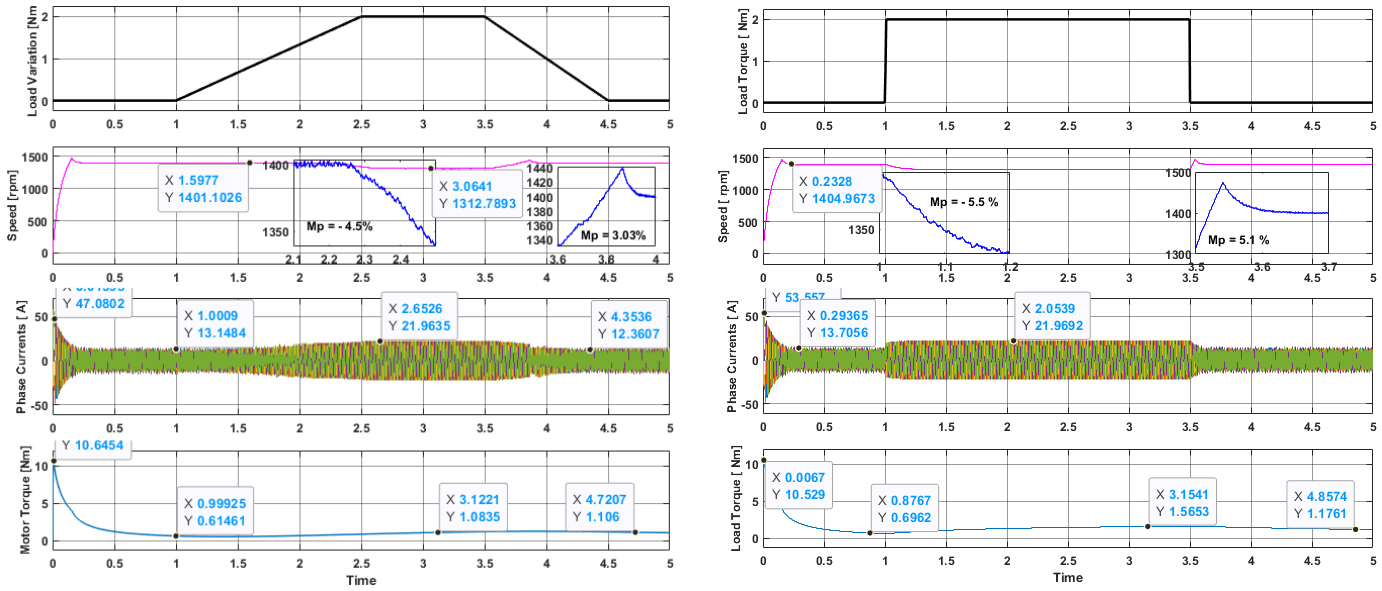


Figure 8. Transient performance of the drive with fuzzy-PI controller.

Table 4. Fuzzy-PI Controller Characteristics.

Load Variation	Characteristics	Time Interval (s)	Overshoot %	Peak Time (s)	Rise Time (s)	Settling Time (s)	Steady State Error
Step load variation	Starting	0–1	4.9	0.1599	0.0993	0.1778	−2 rpm
	Loading	1–1.2	−5.5	1.001	0.1271	1.1950	71 rpm
	Unloading	3.3–3.5	0.2011	3.3146	0.00012	3.499	84 rpm
	Load removal	3.5–5	5.155	3.5404	0.0165	4.999	−2 rpm
Linear load variation	Starting	0–1	4.9	0.1559	0.0993	0.1778	−2 rpm
	Gradual increases of load	1–2.5	−4.5	2.1742	0.1962	2.4980	59 rpm
	Constant Max Load	2.5–3.5	2.25	2.5008	0.1884	3.4988	87 rpm
	Gradual decrease in load	3.5–4.5	3.033	3.8669	0.1992	4.497	1 rpm
	No Load	4.5–5	0.033	4.5778	0.0025	4.999	−1 rpm

4.5. ANFIS-Controller-Driven Drive

The response curves of the proposed drive system with an ANFIS controller for step and gradual changes in load are depicted in Figure 9 and summarized in Table 5.

4.5.1. Starting Characteristics

During the starting of the motor without load, the starting torque rises to 12 nm and settles down at 0.5 nm, with a percentage overshoot of −1.07%, a peak time of 1 s, a rise time of 0.2046 s, and a settling time of 0.5742 s. The steady state starting current is 8.6A (12A for PI, 11A for fuzzy, and 13A for fuzzy-PI) and it is comparatively lower than other controllers. A steady-state error of just 2 rpm is realized.

When the load is linearly increasing from 1 nm to 2 nm between 1 s to 2.5 s, the settling time is 2.49 s, with a 59 rpm steady state error, and a −4.5% (2.1 s to 2.5 s) overshoot. After 2.5 s and up to 3.5 s, when the loading is kept constant at 2 nm, the speed response has a settling time of 3.49 s. Between the time interval of 3.5 s to 4.5 s, the load starts proportionately reducing from 2 nm to 1 nm with an overshoot of 3.03% (14.28% for PI, −0.06% for fuzzy controller), with a 1 rpm error and a settling time 4.49 s. After 4.5 s and until 5 s, the load is completely removed.

4.5.2. Step or Gradual Application and Removal of Load

The performance speed characteristic of instant loading gives a settling time of 1.19 s with a −2.21% overshoot (−3.42% for PI, −0.142% for fuzzy, and −5.5% for fuzzy-PI)

between 1 s to 1.2 s. While unloading, the overshoot is −1% (22.27% for PI, 0.14% for fuzzy and −0.2% for fuzzy-PI) with a settling time of 3.49 s. When the load is proportionately increased from 1 s to 2.5 s to 2 nm, the settling time is 2.422 s with a 16 rpm steady state error (135 rpm for PI, 3 rpm for fuzzy, and 59 rpm for fuzzy-PI), with a −2.42% (1 s to 1.2 s) overshoot.

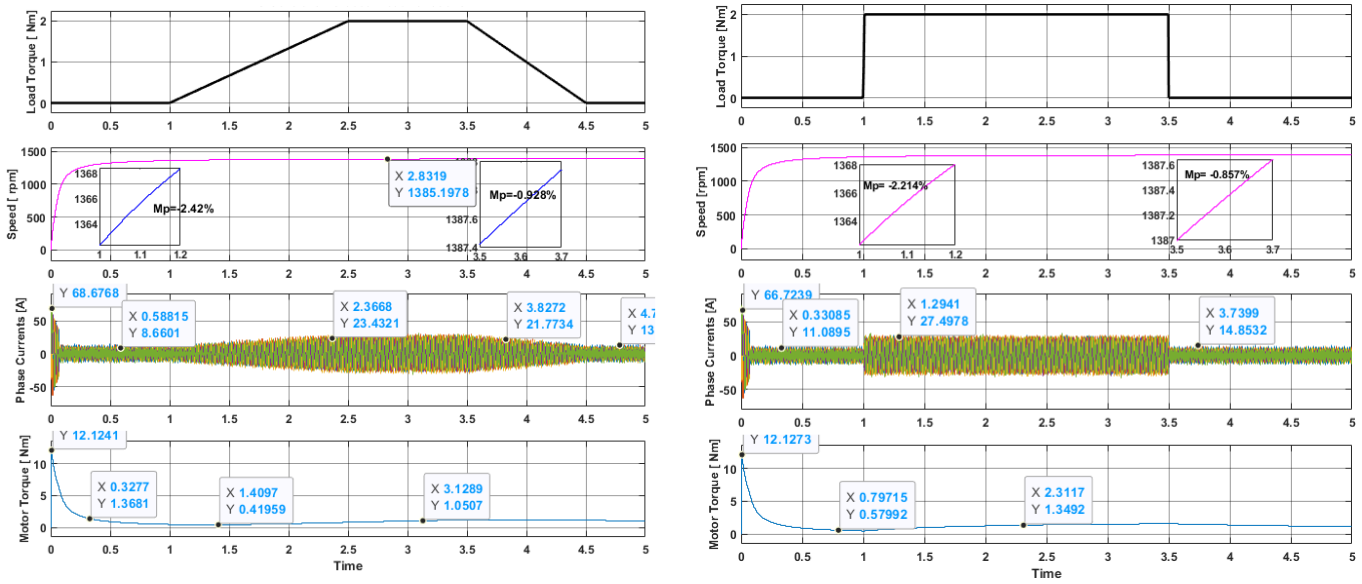


Figure 9. Transient behavior of five-phase PMBLDC motor with ANFIS controller.

Table 5. ANFIS Controller Characteristics.

Load Variation	Characteristics	Time Interval (s)	Overshoot (%)	Peak Time (s)	Rise Time (s)	Settling Time (s)	Steady State Error
Step load variation	Starting	0–1	−1.07	1	0.2046	0.5742	37 rpm
	Loading	1–1.2	−2.214	1.2	0.1599	1.1952	31 rpm
	Unloading	3.3–3.5	−1	3.5	0.1599	3.4957	13 rpm
	Load removal	3.5–5	−0.857	5	1.1858	4.957	9 rpm
Linear load variation	Starting	0–1	−1.07	1	0.2046	0.5742	37 rpm
	Gradual increases of load	1–2.5	−2.42	2.5	1.097	2.422	16 rpm
	Constant Max Load	2.5–3.5	−1.07	3.5	0.7919	3.4720	12 rpm
	Gradual decrease in load	3.5–4.5	−0.928	4.5	0.8014	4.477	10 rpm
	No Load	4.5–5	−0.922	5	0.3996	4.988	9 rpm

After 2.5 s and up to 3.5 s, when loaded to its steady state value of 2 nm, it has a settling time of 3.47 s. Between 3.5 to 4.5 s, the load starts linearly reducing and it decays instantly down with an overshoot of −0.928, a 10 rpm error, and a settling time of 4.47 s. The motor is unloaded after 4.5 s.

The torque speed characteristics of the PMBLDC motor fed from different controllers are shown in Figure 10. It is seen that, for a PI controller, the peak motor torque is 7 nm at a speed of 256 rpm, and settles down at 1400 rpm at 0.9 nm. The torque bandwidth (7 Nm–0.9 nm) is 6.1 nm.

The fuzzy controller gives a peak motor torque of 12.4 nm at a speed of 244 rpm and settles down at 0.6 nm at 1400 prm. The torque bandwidth is 11.8 nm. The fuzzy-PI controller has a torque bandwidth of (10.68-0.6) 10.08 nm. The ANFIS controller has a torque bandwidth of (12.12-1.1) 11.02 nm. The peak torque is high at starting for a fuzzy controller and its bandwidth is more compared with other controllers. The ANFIS controller does not attain a steady state speed and settles at 1390 rpm. Based on the above discussion for high torque requirements, at low speed, such as in electric vehicle applications, the ANFIS controller is preferred, as summarized in Table 6. After a series of jerks, the torque and speed settle down

to their respective final values as the load is removed. The jerk is a perturbation window, which is equal to the step change in speed during load removal. Figure 10 shows the torque speed characteristics of different controllers fed into the PMBLDC drive.

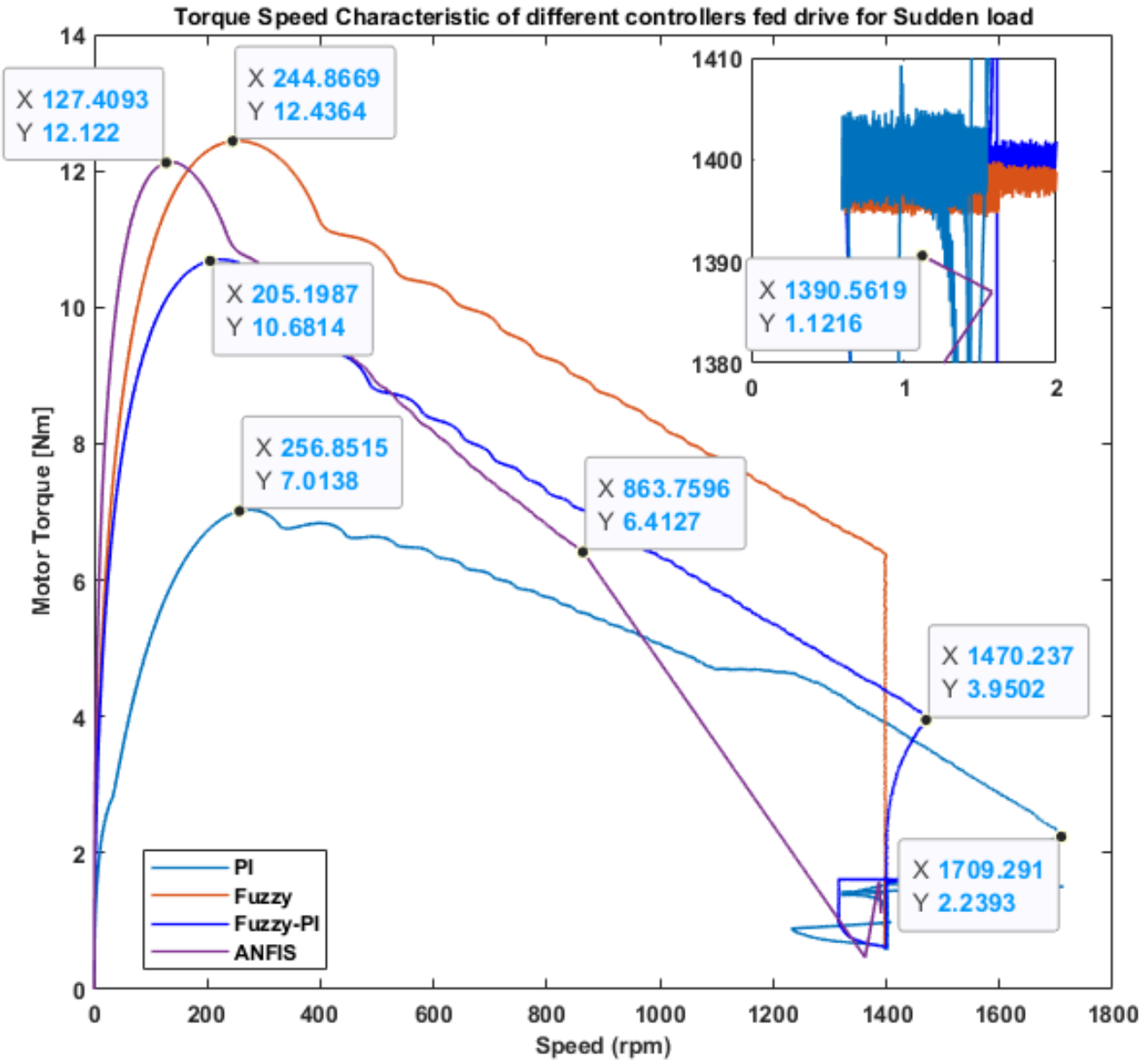


Figure 10. Speed torque characteristics with different controllers.

Table 6. Speed torque comparison of different controllers.

At the Time of	Parameters	PI Controller		Fuzzy Controller				Fuzzy-PI Controller		ANFIS Controller	
		Step Load	Linear Load	Step Load			Linear Load	Step Load	Linear Load	Step Load	Linear Load
Starting	Peak torque (Nm)	7.0	7.0	12.43	12.43	10	10.68	12.11		12.12	
	Speed at peak torque (rpm)	254	256	247	264	220	205	126		127	
Load removal	Maximum speed attained	1708	1710	1398	1399	1471	-	1390		1390	
	jerks (rpm)	1708–1321 (387 rpm)	-	1398–1396 (2 rpm)	-	1347–1399 (52 rpm)	-	1383–1387 (4 rpm)		-	

5. Experiment and Discussions

The designed controllers were experimentally tested with PIC16F870 and PIC16F872 microcontrollers.

The control algorithms of PI, fuzzy, and fuzzy-PI were dumped into the PIC16F872 microcontroller, so that it gave an analog dc voltage from zero to a maximum of 5VDC, as a torque reference command to the PIC16F870 microcontroller. The design values of different controllers were taken from the simulation, and fed as a variable in the controller IC PIC16F872 microcontroller. The component PIC16F872 was a part of the hardware. The primary objective of the PIC16F870 microcontroller is to find the subsequent duty cycle for switching the ten-switch inverter and to perform the commutation. The IRFP260N (MOSFET) is used as a switch for the five-leg, ten-switch voltage source inverter. The hardware setup is depicted in Figure 11. A 24 V switched mode power supply (SMPS) supplying power to a 210 W five-phase PM-BLDC motor through a five-leg inverter is shown. The parameters pertaining to the motor are listed in Table 7. This converter takes any one of the hall inputs and converts the frequency of the hall pulses into corresponding analog voltages.

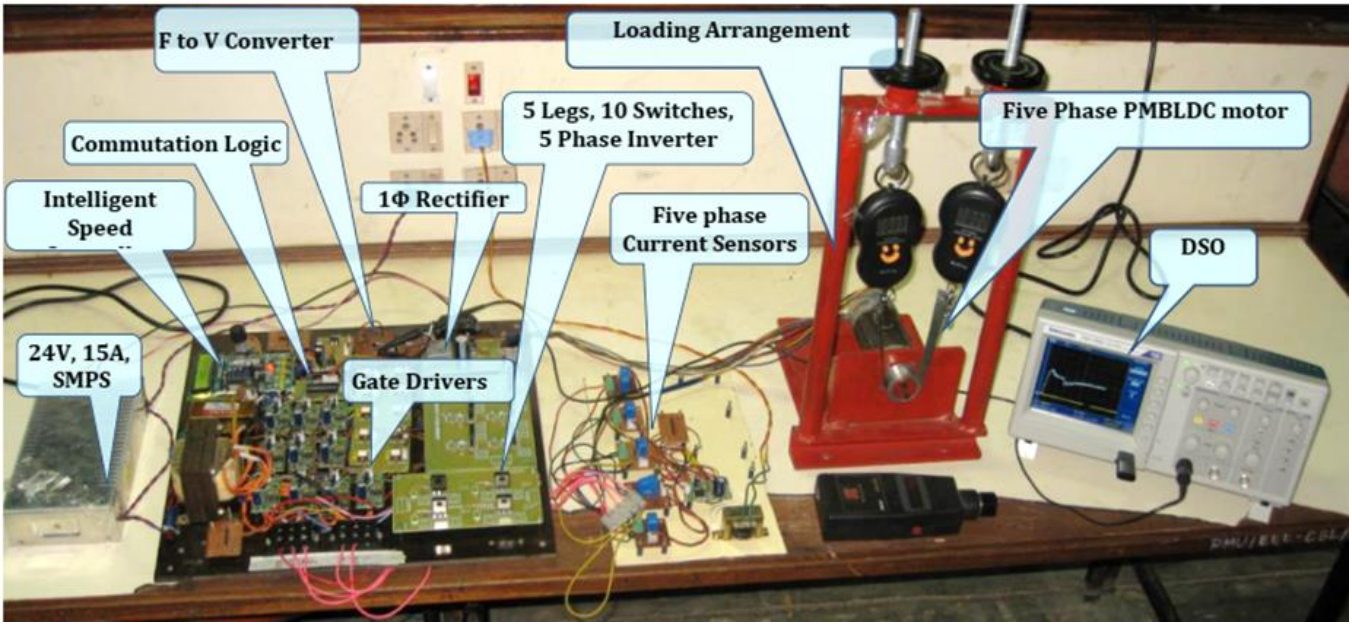


Figure 11. Hardware setup depicting a five-phase intelligent controller-fed PMBLDC drive.

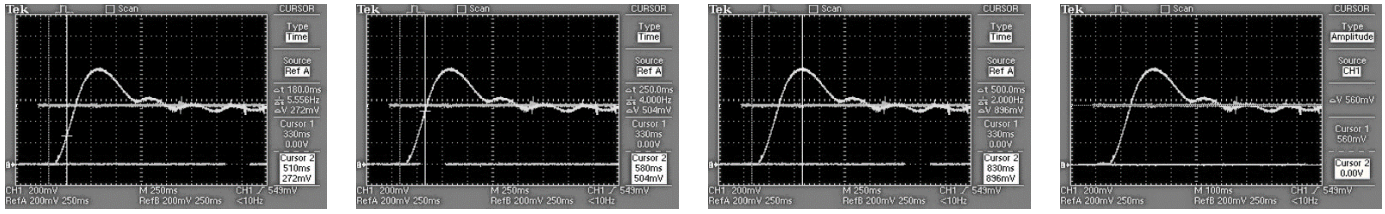
The analog voltage is observed in the digital storage oscilloscope (DSO) as the transient and steady state speed response, as shown in Figures 12–16. To capture the output waveform (Figures 12–16) of the experimental results, a Tektronix two-channel 60 MHz DSO (TBS1062) was used. The F to V converter is standardized such that it generates a dc voltage of 560 mV corresponding to the motor speed of 1400 rpm. The time consumed by the voltage response to reach 50% of the steady state value, i.e., 280 mV, is considered as the delay time and, from Figure 12a, it can be observed that the response takes 180 ms to reach 280 mV.

Table 7. Motor Parameters.

Rated Motor Parameters	Symbol	Value	Units
Power	P	210	Watt
Input Voltage	V_{in}	24	Volt
Armature Current	I_a	10.8	Amps
Rotor speed	N	1500	rpm

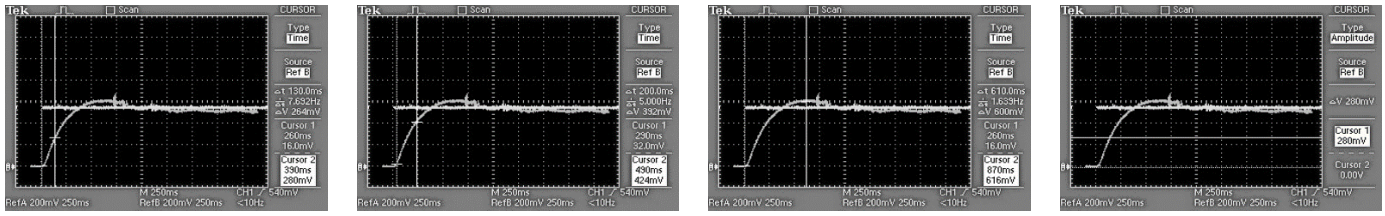
Table 7. *Cont.*

Rated Motor Parameters	Symbol	Value	Units
Per phase resistance	R_a	0.305	ohm
Inductance of Armature	L_a	0.32	mH
Air-gap Flux	Φ	0.02	Wb
Rotor Pole	P	4	-
Torque	T	1.5	Nm
Winding Pattern	-	Delta	-



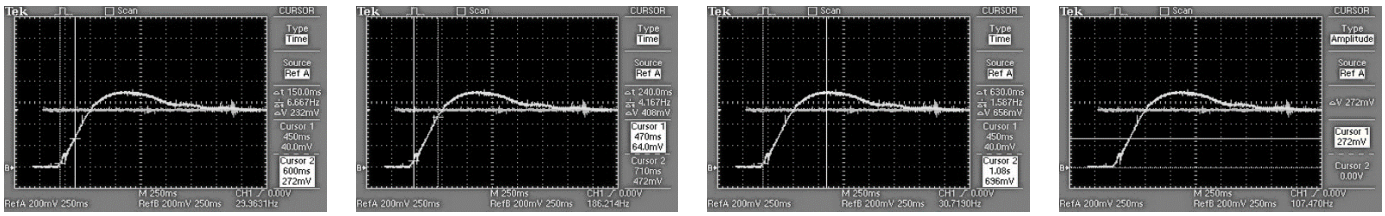
(**a**) (**b**) (**c**) (**d**)

Figure 12. Transient behavior with PI controller (experimental). (**a**) Delay Time, (**b**) Rise Time, (**c**) Peak Time, (**d**) Settle Time.



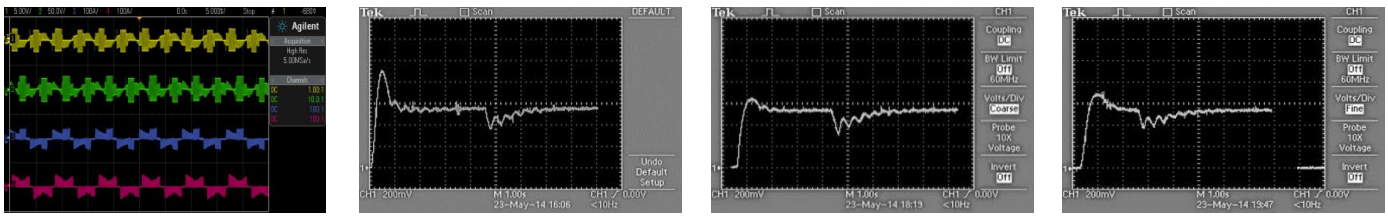
(**a**) (**b**) (**c**) (**d**)

Figure 13. Transient behavior with Fuzzy Controller (Experimental). (**a**) Delay Time, (**b**) Rise Time, (**c**) Peak Time, (**d**) Settle Time.



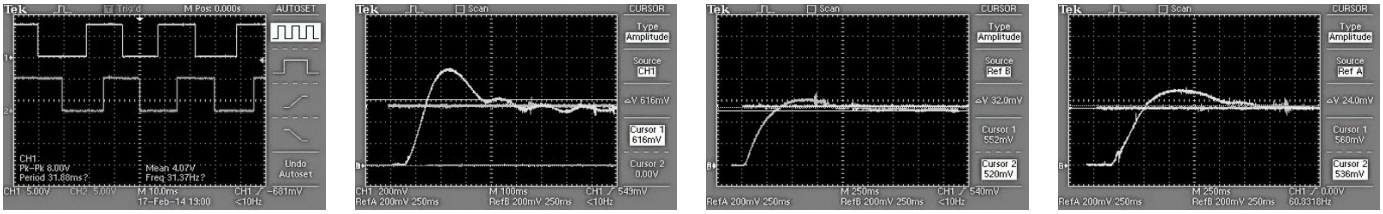
(**a**) (**b**) (**c**) (**d**)

Figure 14. Transient behavior with Fuzzy-PI Controller (Experimental). (**a**) Delay Time, (**b**) Rise Time, (**c**) Peak Time, (**d**) Settle Time.



(**a**) (**b**) (**c**) (**d**)

Figure 15. Five-phase PMBLDC drive waveforms (Experimental). (**a**) Line Voltage Vab, Vbc and Phase-a, Phase-b currents. (**b**) Speed Response of PI Controller fed Drive. (**c**) Speed Response of Fuzzy controller fed Drive. (**d**) Speed response of Fuzzy-PI controller fed Drive.



(**a**) (**b**) (**c**) (**d**)

Figure 16. Overshoot Transient behavior with different controllers (Experimental). (**a**) 72 deg hall displacement at 941.1 rpm. (**b**) Overshoot with PI Controller. (**c**) Overshoot with Fuzzy Controller. (**d**) Overshoot with Fuzzy-PI Controller.

Similar analyses of delay time with fuzzy and fuzzy-PI are depicted in Figures 13a and 14a, respectively. The time taken for a response to reach 90% of the steady state value, i.e., 504 mV, is taken as the rise time and, from Figure 12b, it is observed that the response takes 250 ms to reach 504 mV. Similar analyses of the rise time with fuzzy and fuzzy-PI are shown in Figures 13b and 14b, respectively. The time taken for a response to reach its maximum amplitude for the first time is 500 ms to reach 896 mV. Similar analyses of the peak time with fuzzy and fuzzy-PI are shown in Figures 13c and 14c, respectively. This peak value of 896 mV corresponds to 2240 rpm of the motor during its transient period. The time taken for a response to settle within 3 to 5% of its steady state value is taken as the settling time and, from Figure 12d, it is observed that the response takes 270 ms to reach 560 mV. Similar analyses of peak time with fuzzy and fuzzy-PI are depicted in Figures 13d and 14d, respectively.

The waveforms in Figure 15a are taken from the Agilent four-channel DSO (x-3034A model) with a 10:1 probe for measuring line voltages and a 100:1 probe for measuring phase currents, respectively. The first two channels give the line-to-line voltage (V_{ab} and V_{bc}) and the next two channels give the two phase currents (Ia and I_b). A 2.4 V peak-to-peak voltage corresponds to a 24 V peak-to-peak voltage in a probe ratio of 10:1. Similarly, a 34 mA peak-to-peak current with a 100:1 probe ratio gives a 3.4 A phase current. Figure 15b–d is taken from the Tektronix two-channel 60 MHz DSO (TBS1062). The hall signals received from the motor are connected to an F to V (Frequency to Voltage) converter to obtain an analog voltage corresponding to the frequency of the hall element. The F to V converter is calibrated for a 560 mv output voltage at a speed of 1400 rpm. The frequency of the hall element is directly proportional to the speed of the BLDC motor; with a different controller algorithm, the speed responses for different controllers in terms of step load variation are taken and depicted in Figure 15b–d.

As seen in Figure 15b, the motor is started with no load and, after 2.7 s, the motor reaches a steady state speed of 1400 rpm (560 mV) with an overshoot of 37.8% (900 mV). At a time of 4.6 s, a load of 1.5 nm is applied. It is observed that the motor speed immediately drops after applying the load and, due to PI controller action, the steady state speed is restored in 7 s. Figure 15c shows the steady state and transient performance of the fuzzy controller. The motor initially starts with zero load and subsequently reaches a steady state speed of 1400 rpm in less than 1 s. A step load of 1.5 nm is applied at 3.8 s. The controller reverts the motor back to its rated speed in less than a second. When compared to the PI controller, the overshoot percentage is negligible.

The motor attains a steady-state speed quicker compared to the PI controller. The transient and steady state response of the adaptive hybrid fuzzy-PI controller is shown in Figure 15d, showing that the motor starts at no load and reaches a speed of 1400 rpm in less than 1.6 s. At 2.4 s, a step load disturbance of 1.5 nm is applied, and it is observed that the controller reaches a rated speed of 1400 rpm in less than two seconds.

There are five hall sensors mounted on the rotor with a 36° magnetic angle or 72° electrical angle to alter the rotor position of the five-phase PMBLDC motor. Figure 16a gives the phase displacement of two-hall sensor pulses at a speed of 941 rpm. The total

time period for one pulse is 31.88 ms or 15 divisions. We can see that the time displacement between the two-hall pulses is three divisions, as it corresponds to a 72° displacement between the hall sensor pulses.

Figure 16 b–d present the overshoot responses for the three controllers, namely, PI, fuzzy, and fuzzy-PI. To measure the overshoot response, the machine is started with no load and waveforms are captured until the machine attains a steady state speed (1400 rpm). In Figure 16b, it can be observed that the response oscillates between 616 mV and 512 mV before attaining its steady state value of 560 mV. These oscillations are taken as the overshoot of the response. It accounts for a ± 37.8% oscillation from the steady state value. Similar analyses of overshoot with fuzzy and fuzzy-PI are shown in Figures 16c and 16d, respectively. It is observed that, from the above analysis, the experimental performance of the fuzzy controller is superior to the other two controllers, as shown in Table 8.

Table 8. Comparison of PI, Fuzzy, and Adaptive Hybrid Fuzzy-PI Controllers (Experiment).

Controller	Delay Time (sec)	Rise Time (sec)	Peak Time (sec)	Percentage Overshoot (%)	Settling Time (sec)	Torque Ripple (Nm)
PI	0.18	0.25	0.5	37.5	2.5	0.49
Fuzzy	0.13	0.2	0.61	8	1	0.04
Hybrid Fuzzy-PI	0.15	0.24	0.63	19.54	1.5	0.38

Due to the high inertia of the motor, the experimental investigation was only carried out for the step load variation, while another simulation was carried out for both step and linear load variations. In the simulation, the time domain specification for both torque and speed is investigated, while in the experimental results, a time domain investigation is only carried out for the motor speed for step load variation. The comparison between simulation and experimental results is tabulated in Table 9.

Table 9. Comparison of different controllers (Simulation and Experiment).

Controllers	Delay Time (sec)		Rise Time (sec)		Peak Time (sec)		Percentage Overshoot (%)		Settling Time (sec)		Torque Ripple (Nm)	
	Experimental Value	Simulated Value	Experimental Value	Simulated Value	Experimental Value	Simulated Value	Experimental Value	Simulated Value	Experimental Value	Simulated Value	Experimental Value	Simulated Value
PI	0.18	0.04	0.25	0.10	0.5	0.324	37.5	20.19	2.5	4.07	0.49	1.72
Fuzzy	0.13	0.03	0.2	0.07	0.61	0.096	8	0.334	1	0.09	0.04	2
Hybrid Fuzzy-PI	0.15	0.038	0.24	0.104	0.63	0.168	19.54	5.127	1.5	0.19	0.38	2
ANFIS	-	0.03	-	0.05	-	0.07	-	0.217	-	0.06	-	0.06

6. Conclusions

The selection of compatible motor drive systems and controllers for electric vehicle applications pertaining to steady and intermittent loads is urgently needed, and this work precisely caters to this requirement. The dynamic characteristics of the five-phase PMBLDC drive system with conventional fuzzy, PI, adaptive hybrid-fuzzy-PI, and ANFIS controllers for step loading conditions and linear loading conditions were simulated, and their time domain specifications were compared in this research. The step loading conditions were experimentally carried out for PI, fuzzy, and fuzzy- PI (Hybrid), and similar time domain analyses were compared. It was found that, among the four controllers used in the simulations, the ANFIS controller gave a better dynamic response, while in

the experimental validation among the three other controllers, the fuzzy controller gave a much-improved dynamic response to the overall system. The controller characteristics were compared in terms of rise time, delay time, percentage overshoot, peak time, starting torque, settling time, and torque ripple. Hardware results based on the ANFIS controller will be considered for future research. Moreover, the impact of different drive cycles for EV applications on the time response can be investigated in the future.

Author Contributions: Conceptualization, M.A.I. and N.S.; Methodology, M.A.I., N.S. and A.B.; Proposed Architectures Designing and Implementation: M.A.I. and N.S.; Software, M.A.I., N.S., R.A. and S.A.; Validation, M.A.I., R.A. and S.A.; Formal Analysis, M.A.I. and N.S.; Investigation, M.A.I., N.S. and A.B.; Resources, R.A. and S.A.; Data Curation, M.A.I. and N.S.; Writing—original draft preparation, M.A.I., N.S., A.B., R.A. and S.A.; Writing—review and editing, M.A.I. and A.B.; Visualization, M.A.I., N.S. and A.B.; Supervision, M.A.I.; Project Administration, M.A.I. and N.S. All authors have read and agreed to the published version of the manuscript.

Funding: This research received no external funding.

Institutional Review Board Statement: Not applicable.

Informed Consent Statement: Not applicable.

Data Availability Statement: The data used to support the findings of this study are included in the article. Should further data or information be required, these are available from the corresponding author upon request.

Conflicts of Interest: The authors declare no conflict of interest.

References

1. Henderson, J.R.; Miller, J.E. *Design of Brushless Permanent Magnet Motor*; Motor Design Books LLC: Venice, FL, USA, 1994.
2. Duran, M.J.; Gonzalez-Prieto, I.; Gonzalez-Prieto, A.; Aciego, J.J. The Evolution of Model Predictive Control in Multiphase Electric Drives: A Growing Field of Research. *IEEE Ind. Electron. Mag.* **2022**, *16*, 29–39. [CrossRef]
3. Khamitov, A.; Severson, E.L. Analysis and design of multi-phase combined windings for bearingless machines. In Proceedings of the 2021 IEEE Energy Conversion Congress and Exposition (ECCE), Vancouver, BC, Canada, 10–14 October 2021; pp. 3949–3956.
4. Wei, Y.; Qiao, M.; Zhu, P. Fault-Tolerant Operation of Five-Phase Permanent Magnet Synchronous Motor with Independent Phase Driving Control. *CES Trans. Electr. Mach. Syst.* **2022**, *6*, 105–110. [CrossRef]
5. Wu, Y.; Zhang, Z.; Li, Y.; Sun, Q. Open-circuit fault diagnosis of six-phase permanent magnet synchronous motor drive system based on empirical mode decomposition energy Entropy. *IEEE Access* **2021**, *9*, 1137–1147. [CrossRef]
6. Xiong, C.; Xu, H.; Guan, T.; Zhou, P. A constant switching frequency multiple-vector-based model predictive current control of five-phase PMSM with nonsinusoidal back EMF. *IEEE Trans. Ind. Electron.* **2019**, *67*, 1695–1707. [CrossRef]
7. Harikrishnan, P.; Pandey, P.; Titus, J.; Hatua, K. Fault Tolerant Operation of an LCI and VSI fed Hybrid Induction Machine Drive for Medium Voltage High Power Applications. In Proceedings of the IEEE Energy Conversion Congress and Exposition (ECCE), Detroit, MI, USA, 9–13 October 2022; pp. 1–7.
8. Kammermann, J.; Bolvashenkov, I.; Herzog, H.G.; Brazhnikov, A.V. Design Features and Benefits of Advanced Multiphase Inverter-Fed Electric Drives. In Proceedings of the Second International IEEE Conference on Sustainable Mobility Applications, Renewables and Technology (SMART), Cassino, Italy, 23–25 November 2022; pp. 1–7.
9. Sun, X.; Liu, Z.; Jiang, D.; Li, A.; Wang, P.; Qu, R. Switch Short-Circuit Fault-Tolerant Control of Five-Phase Open-Winding Motor Drive with a Floating Capacitor. *IEEE Trans. Ind. Electron.* **2022**, 1–11. [CrossRef]
10. Huang, J.; Sui, Y.; Yin, Z.; Yang, S.; Zheng, P. Five-Phase Hybrid Single-/Double-Layer Fractional Slot-Winding PMSM for Torque Improvement Under Third Harmonic Current Injection Condition. *IEEE Trans. Magn.* **2022**, *58*, 1–6. [CrossRef]
11. Zhou, Y.; Liu, M.-S.; Hu, L.-S.; Zhang, Z.-D. Application of fuzzy five states control system base on phase plane in steer by wire system of loader. In Proceedings of the Seventh International Conference on Fuzzy Systems and Knowledge Discovery (FSKD), Yantai, China, 10–12 August 2010; pp. 10–12.
12. Islam, M.T.; Islam, M.S. Design and optimization of a self-tuning PID controller based on Fuzzy Logic for Temperature Control System of Furnace. In Proceedings of the International IEEE Conference on Electronics, Communications and Information Technology (ICECIT), Khulna, Bangladesh, 14–16 September 2021; pp. 1–4.
13. De Viaene, J.; Ceulemans, D.; Derammelaere, S.; Stockman, K. Sensorless load angle control for energy optimal sinusoidal driven BLDC motor applications. *IEEE/ASME Trans. Mechatron.* **2021**, *27*, 2290–2300. [CrossRef]
14. Du, Y.; Ji, J.; Zhao, W.; Tao, T.; Xu, D. Self-adapted model predictive current control for five-phase open-end winding PMSM with reduced switching loss. *IEEE Trans. Power Electron.* **2022**, *37*, 11007–11018. [CrossRef]
15. Menon, M.; Jacob, B. A New Space Vector Pulse Density Modulation Scheme for Two-Level Five Phase Induction Motor Drive. *IEEE Trans. Ind. Electron.* **2022**, *69*, 12077–12085.

16. Reddy, V.S.; Devabhaktuni, S. Enhanced Low-Speed characteristics with Constant Switching Torque Controller-based DTC Technique of Five-Phase Induction Motor Drive with FOPI Control. *IEEE Trans. Ind. Electron.* **2022**, *12*, 1–10. [CrossRef]
17. Iffouzar, K.; Amrouche, B.; Cherif, T.O.; Benkhoris, M.-F.; Aouzellag, D.; Ghedamsi, K. Improved direct field oriented control of multiphase induction motor used in hybrid electric vehicle application. *Int. J. Hydrogen Energy* **2017**, *42*, 19296–19308. [CrossRef]
18. Park, H.; Kim, T.; Suh, Y. Fault-Tolerant Control Methods for Reduced Torque Ripple of Multiphase BLDC Motor Drive System Under Open-Circuit Faults. *IEEE Trans. Ind. Appl.* **2022**, *8*, 7275–7285. [CrossRef]
19. Echeikh, H.; Trabelsi, R.; Iqball, A.; Mimouni, M.F. Real time implementation of indirect rotor flux oriented control of a five-phase induction motor with novel rotor resistance adaption using sliding mode observer. *J. Frankl. Inst.* **2018**, *355*, 2112–2141. [CrossRef]
20. Chikondra, B.; Muduli, U.R.; Behera, R.K. Improved DTC technique for THL-NPC VSI fed five-phase induction motor drive based on VVs assessment over a wide speed range. *IEEE Trans. Power Electron.* **2021**, *37*, 1972–1981. [CrossRef]
21. Chhlonh, C.; Kim, B.; Chrin, P.; Am, S.; Seng, T. Four in-wheel bldc motors speed control in EV based on hybrid fuzzy-pi controller visual on GUI. In Proceedings of the International Symposium on Electrical and Electronics Engineering (ISEE), Ho Chi Minh, Vietnam, 15–16 April 2021; pp. 166–171.
22. El-Zohri, E.H.; Mosbah, M.A. Speed control of inverter-fed induction motor using hybrid fuzzy-PI controller. In Proceedings of the International IEEE Conference on Innovative Trends in Communication and Computer Engineering (ITCE), Aswan, Egypt, 8–9 February 2020; pp. 216–221.
23. Mazibukol, N.; Akindejil, K.T.; Sharma, G. Implementation of a FUZZY logic controller (FLC) for improvement of an Automated Voltage Regulators (AVR) dynamic performance. In Proceedings of the IEEE Power Electronic Society/IAS PowerAfrica, Kigali, Rwanda, 22–26 August 2022; pp. 1–5.
24. Murdianto, F.D.; Ashari, M. Comparison of ANFIS and FLC for CC-CV Precise Charging. In Proceedings of the International IEEE Seminar on Intelligent Technology and Its Applications (ISITIA), Surabaya, Indonesia, 20–21 July 2022; pp. 395–400.
25. Suhail, M.; Akhtar, I.; Kirmani, S.; Jameel, M. Development of progressive fuzzy logic and ANFIS control for energy management of plug-in hybrid electric vehicle. *IEEE Access* **2021**, *9*, 62219–62231. [CrossRef]
26. Guo, Y.; Mohamed, M.E. Speed control of direct current motor using ANFIS based hybrid PID configuration controller. *IEEE Access* **2020**, *8*, 125638–125647. [CrossRef]
27. Baidya, D.; Dhopte, S.; Bhattacharjee, M. Sensing System Assisted Novel PID Controller for Efficient Speed Control of DC Motors in Electric Vehicles. *IEEE Sens. Lett.* **2023**, *7*, 6000604. [CrossRef]
28. Liu, F.; Wang, H.; Shi, Q.; Wang, H.; Zhang, M.; Zhao, H. Comparison of an ANFIS and fuzzy PID control model for performance in a two-axis inertial stabilized platform. *IEEE Access* **2017**, *5*, 12951–12962. [CrossRef]
29. Tariq, M.; Bhattacharya, T.K.; Varshney, N.; Rajapan, D. Fast response Antiwindup PI speed controller of Brushless DC motor drive: Modeling, simulation and implementation on DSP. *J. Electr. Syst. Inf. Technol.* **2016**, *3*, 1–13. [CrossRef]
30. Mohanraj, D.; Gopalakrishnan, J.; Chokkalingam, B.; Mihet-Popa, L. Critical Aspects of Electric Motor Drive Controllers and Mitigation of Torque Ripple-Review. *IEEE Access* **2022**, *10*, 73635–73674. [CrossRef]
31. Kumar, D.; Gupta, R.A.; Gupta, N. Modelling and simulation of four switch three-phase BLDC motor using anti-windup PI controller. In Proceedings of the IEEE Innovations in Power and Advanced Computing Technologies (i-PACT), Vellore, India, 21–22 April 2017; pp. 1–6.
32. Ziegler, J.G.; Nichols, N.B. Optimum setting for automatic controllers. *ASME Trans.* **1942**, *64*, 759–768. [CrossRef]
33. Do, C.P.; Le, D.K. Improved of Dynamic Torque by Field Oriented Control based Fuzzy Logic for BLDC Motor. In Proceedings of the IEEE 7th National Scientific Conference on Applying New Technology in Green Buildings (ATiGB), Da Nang, Vietnam, 11–12 November 2022; pp. 92–97.
34. Tripathy, S.N.; Kundu, S.; Pradhan, A. Modelling of Dynamic Fuzzy-PID based Speed Controller for BLDC Motor. In Proceedings of the 1st IEEE International Conference on Industrial Electronics: Developments & Applications (ICIDeA), Bhubaneswar, India, 15–16 October 2022; pp. 110–115.
35. Rifai, A.F.; Rudiansyah, H.; Milanto, R. Design and Implementation of Auto-limit Riding Speed System for Electric Motorcycles Based on Battery Level with Fuzzy PID. In Proceedings of the 7th IEEE International Conference on Electric Vehicular Technology (ICEVT), Bali, Indonesia, 14–16 September 2022; pp. 27–33.
36. Vellingiri, M. Design of Shell Game Optimization based Adaptive Neuro Fuzzy Controller for Brushless DC Drives Lifetime Maximization. In Proceedings of the Third International IEEE Conference on Inventive Research in Computing Applications (ICIRCA), Coimbatore, India, 2–4 September 2021; pp. 205–212.
37. Zhai, R.; Xiao, P.; Zhang, R.; Ju, J. In-wheel motor control system used by four-wheel drive electric vehicle based on whale optimization algorithm-proportional–integral–derivative control. *Adv. Mech. Eng.* **2022**, *14*, 1–16. [CrossRef]
38. Pal, S.; Patel, A.; Jabade, A.M.; Miduthuru, K.; Sahu, G.; Botre, B.A.; Verma, B.K.; Akbar, S.A. Parameter Estimation and Comparative Analysis of Control Design Techniques for BLDC Hub Motor. In Proceedings of the 17th IEEE India Council International Conference (INDICON), New Delhi, India, 10–13 December 2020; pp. 1–8.
39. Rahimi, T.; Ding, L.; Peyghami, S.; Kheshti, M.; Blaabjerg, F.; Davari, P. Time domain simulation of a five-phase BLDC motor drive. In Proceedings of the 11th IEEE Power Electronics, Drive Systems, and Technologies Conference (PEDSTC), Tehran, Iran, 4–6 February 2020; pp. 1–6.

40. Inayathullaah, M.A.; Anita, R. Experimental Evaluation of Fuzzy Logic Based Five Phase PMBLDC Motor Drive. *Int. Rev. Electr. Eng.* **2014**, *5*, 757–763. [CrossRef]
41. Hidayat, H.; Sasongko, P.H.; Sarjiya, S.; Suharyanto, S. Performance analysis of Adaptive Neuro Fuzzy Inference Systems (ANFIS) for speed control of brushless DC motor. In Proceedings of the International IEEE Conference on Electrical Engineering and Informatics (ICEEI), Bandung, Indonesia, 7–19 July 2011; pp. 1–6.

Disclaimer/Publisher's Note: The statements, opinions and data contained in all publications are solely those of the individual author(s) and contributor(s) and not of MDPI and/or the editor(s). MDPI and/or the editor(s) disclaim responsibility for any injury to people or property resulting from any ideas, methods, instructions or products referred to in the content.